EUKARYOTIC CELL, Oct. 2006, p. 1674–1687 Vol. 5, No. 10
1535-9778/06/$08.00+0 doi:10.1128/EC.00252-06

TOS9 Regulates White-Opaque Switching in *Candida albicans*▽†

Thyagarajan Srikantha,[1] Anthony R. Borneman,[2] Karla J. Daniels,[1] Claude Pujol,[1] Wei Wu,[1] Michael R. Seringhaus,[3] Mark Gerstein,[3] Song Yi,[1] Michael Snyder,[2] and David R. Soll[1]*

Department of Biological Sciences, The University of Iowa, Iowa City, Iowa 52242,[1] and Department of Molecular, Cellular, and Developmental Biology[2] and Department of Molecular Biophysics and Biochemistry,[3] Yale University, New Haven, Connecticut 06511

Received 7 August 2006/Accepted 18 August 2006

In *Candida albicans*, the a1-α2 complex represses white-opaque switching, as well as mating. Based upon the assumption that the a1-α2 corepressor complex binds to the gene that regulates white-opaque switching, a chromatin immunoprecipitation-microarray analysis strategy was used to identify 52 genes that bound to the complex. One of these genes, *TOS9*, exhibited an expression pattern consistent with a "master switch gene." *TOS9* was only expressed in opaque cells, and its gene product, Tos9p, localized to the nucleus. Deletion of the gene blocked cells in the white phase, misexpression in the white phase caused stable mass conversion of cells to the opaque state, and misexpression blocked temperature-induced mass conversion from the opaque state to the white state. A model was developed for the regulation of spontaneous switching between the opaque state and the white state that includes stochastic changes of Tos9p levels above and below a threshold that induce changes in the chromatin state of an as-yet-unidentified switching locus. *TOS9* has also been referred to as *EAP2* and *WOR1*.

White-opaque switching was first observed in a strain of *Candida albicans* isolated from a fatal bloodstream infection (40). The switch affected the cellular phenotype (1, 41, 42), gene expression (24), and a variety of putative virulence traits (40, 41). It also conferred the capacity to colonize skin (23). An early analysis of clinical strains performed in 1986, however, revealed that only 8% underwent the switch (D. R. Soll, unpublished observation; 44). This observation was enigmatic, since all strains of *C. albicans* possessed opaque state-specific genes (33). In 2002, Miller and Johnson (31) provided not only an explanation for this enigma but also a role for the white-opaque transition. They found that while an **a**/α laboratory strain could not switch, *MTL***a**1 and *MTL*α2 deletion derivatives of that strain, which were α and **a**, respectively, could. They demonstrated that switching in the **a**/α strain was repressed by the **a**1-α2 complex, the same complex that repressed mating (31). Their results suggested that in order to switch, natural strains, which are predominantly **a**/α (26, 30, 48), first had to undergo homozygosis to **a**/**a** or α/α. Lockhart et al. (30) generalized this observation by demonstrating that while natural **a**/α strains did not undergo white-opaque switching, spontaneously generated *MTL*-homozygous offspring and natural *MTL*-homozygous strains did switch. Miller and Johnson (31) further demonstrated that in order to mate, the **a** and α strains they derived by deleting *MTL*α2 and *MTL***a**1, respectively, first had to switch from white to opaque. Lockhart et al. (29) generalized this observation by demonstrating that only natural **a**/**a** and α/α strains that expressed the opaque phenotype could mate. The white-opaque transition, therefore, was an essential and unique step in the *C. albicans* mating process (3, 42, 43).

In spite of the fundamental role white-opaque switching plays in mating, very little is known about the molecular mechanisms that regulate it. Because white-opaque switching occurs spontaneously, reversibly, and at relatively high frequency, it has been suggested (21, 41, 42, 46) that it may be the result of "position-effect variegation," a metastable change in the expression of a gene, mediated by a change in chromatin state effected by a neighboring silent region (12, 20, 28). This hypothesis was supported by the observation that the deacetylase inhibitor trichostatin A or deletion of the deacetylase gene *HDA1* or *RPD3* caused increases in the frequency of white-opaque switching (21, 46). Directly testing this hypothesis, however, requires identification of the site of the switching event. Since the **a**1-α2 complex represses white-opaque switching (31), we hypothesized that it may bind upstream of a genomic switch site, which we will refer to for the sake of discussion as the "master switch gene" (MSG). We therefore used a chromatin immunoprecipitation-microarray analysis (ChIP-chip) strategy (18, 35) to identify **a**1-α2 binding sites throughout the *C. albicans* genome, analyzed the transcription profiles of the genes associated with **a**1-α2 binding sites to identify candidate genes for either the MSG or an MSG activator, and finally tested the role of candidate genes in switching by mutant analysis. We present here the repertoire of genes that are bound by the **a**1-α2 repressor complex, transcription profiles of these genes, and mutant analyses that test the role of candidate genes in switching. Our analysis has identified one gene, *TOS9*, which exhibits characteristics consistent with an MSG.

MATERIALS AND METHODS

Strain maintenance. For the strains used in this study, as well as their origins and genotypes, see Table S1 in the supplemental material. For experimental purposes, cells were plated at 25°C on agar containing either modified Lee's

* Corresponding author. Mailing address: Department of Biological Sciences, 302 BBE, The University of Iowa, Iowa City, IA 52242. Phone: (319) 335-1117. Fax: (319) 335-2772. E-mail: david-soll@uiowa.edu.

† Supplemental material for this article may be found at http://ec.asm.org/.

▽ Published ahead of print on 1 September 2006.

medium (2, 25) or YPD medium (38). Clones were then picked and grown in the same liquid medium at 25°C.

Generation of Myc-tagged strains. Strains were generated harboring the 13× Myc epitope tag at either *MTL***a**1 or *MTL*α2. The **a**1p and α2p transformation modules containing the Ca*URA3* gene were generated by PCR with pURA3 RV-13 DNA as the template (A. R. Borneman and M. Snyder, unpublished results) and the 80-mer C-terminal tagging primers **A**1RVF2 and **A**1RVR1 for *MTL***a**1p and primers P2RVF2 and P2RVR1 for *MTL*α2p (see Table S2 in the supplemental material). *ura3*$^-$ **a**/α strain CAI4 (10) was transformed with either module, and two **a**1-Myc-tagged strains (**a**1-29.1 and **a**1.29.2) and four α2-Myc-tagged strains (α2-3.1, α2-3.2, α2-4.1, and α2-8.1) were verified by PCR for correct in-frame fusion and the number of Myc units and by Western analysis for protein levels.

ChIP-chip analyses. A whole-genome tiled-oligonucleotide array was used that contained 246,532 oligonucleotides 50 nucleotides in length, generated at a 60-bp spacing (10 bp between adjacent oligonucleotides) spanning the Watson strand of assembly 19 of the *C. albicans* genome (19). In addition, 123,271 oligonucleotides 50 nucleotides in length were designed at a 120-bp spacing (70 bp between adjacent oligonucleotides) to span the Crick strand. The start positions for the oligonucleotides on the Crick strand were generated with a 30-bp offset relative to those on the Watson strand. Arrays were synthesized on microarray slides by maskless photolithography (Nimblegen LLC, Iceland). The array design has been deposited in the Gene Expression Omnibus (GEO; http://www.ncbi.nlm.nih.gov/geo/) under platform number GPL4037.

For analysis, cells were grown in modified Lee's medium. ChIP and DNA labeling were performed as described for *Saccharomyces cerevisiae* (5). Hybridization was performed according to the manufacturer's (Nimblegen LLC) protocols.

The array data from three independent immunoprecipitations for each of the **a**1p::Myc and α2p::Myc strains were used for the analysis of binding. Following array scanning, the two files corresponding to Cy3 and Cy5 channels in pair file format were uploaded to the Tilescope pipeline for high-density filing array analysis (http://tilescope.gersteinlab.org; H. Zhang et al., submitted for publication) by quantile normalization with a window size of 400 bp, a MaxGap (the maximum gap allowed between probes above threshold) of 60 bp, and a MinRun (the minimum length of the region with probes above the threshold) of 120 bp. Regions corresponding to the putative transcription factor binding site were determined with thresholds for both the signal (pseudomedian signal, ≥1.15) and the *P* value ($P < 1 \times 10^{-4}$). Regions corresponding to the putative transcription factor binding sites were determined with thresholds for both the signal (pseudomedian signals, ≥1.15) and the *P* value ($P < 1 \times 10^{-4}$). All of the raw data files for each experiment have been deposited in GEO under series number GSE5493.

Anti-Myc immunoprecipitation of *CAG1*. To test whether the Myc-tagged **a**1-α2 complex bound to a known target, cells of Myc-tagged strains **a**1-29.1 and α2-3.1 were lysed (16) and the supernatant was subjected to sonication to obtain sheared chromatin averaging 500 to 800 bp in length. The sheared chromatin was incubated with either an anti-Myc monoclonal antibody (9E10) or a control anti-neuron monoclonal antibody (22C10) (Developmental Studies Hybridoma Bank, Iowa City, Iowa) at 4°C overnight. DNA was then extracted and used for PCR amplification of the *CAG1* promoter region that spanned the **a**1-α2 binding site (17). PCR amplification was performed with primers CAGPr1and CAGPr2 (see Table S2 in the supplemental material).

Northern analysis. Northern analyses were performed with either poly(A)$^+$ mRNA or total RNA obtained from cells of **a**/α strain CAI4, white and opaque cells of α/α strains WO-1 and WUM5A, and white and opaque cells of **a**/**a** strain P37005. For the primers used to generate the PCR probes for Northern analysis of 51 genes identified by ChIP-chip analysis, see Table S2 in the supplemental material. Northern blot hybridization was performed as previously described (9).

Generation of *TOS9* and *PSO2* null mutants. Recyclable nourseothricin resistance (SAT^r) cassettes I and II, based on the maltose-inducible flipper, were used to create null mutants of *TOS9* and *PSO2* in *ura3*$^-$ strain WUM5A, a derivative of α/α strain WO-1 (36, 47). The plasmid containing the SAT^r cassette and strain WUM5A were generous gifts from Joachim Morschhäuser, University of Würzburg. Deletion cassette I was generated as described below. Primers TOS9f1 and TOS9r1 were used to generate a 650-bp 5′-flanking region of *TOS9*, and primers TOS9f2 and TOS9r2 were used to generate a 600-bp 3′-flanking region (see Table S2 in the supplemental material). PCR products were used to generate a 5′-3′ fusion that contained the SAT^r marker and lacked the entire *TOS9* open reading frame (ORF). Deletion cassette I harboring this *TOS9* deletion construct was then used to transform WUM5A (36, 47). Two independent transformants, TOHE1 and TOHE3, were verified as heterozygous deletion derivatives and subjected to a POP-OUT protocol to excise the recyclable SAT^r cassette. The second allele was disrupted in TOHE3POP2, a pop-out clone of Tohe3, with deletion cassette II. Deletion cassette II included a 350-bp 5′-flanking region generated with primers Tos9f3 and Tos9r3 and a 300-bp 3′-flanking region generated with primers Tos9f4 and Tos9r4 (see Table S2 in the supplemental material). It lacked the 1,732-bp *TOS9* ORF. The second round of disruption resulted in *TOS9* null mutant TOHO3. *PSO2* null mutant PSHO1 was generated in a similar fashion with independent deletion cassettes I and II. For cassette I, primers PSO2f1 and PSO2r1 were used to generate a 5′-flanking region and primers Psof2 and Psor2 were used to generate a 3′-flanking region (see Table S2 in the supplemental material). For cassette II, primers 5362f3 and 5362r3 were used to generate a 5′-flanking region and primers 5362f4 and 5362r4 were used to generate a 3′-flanking region (see Table S2 in the supplemental material).

Generation of GFP-tagged *TOS9* mutant strains. *TOS9* 5′- and 3′-flanking DNA was generated by PCR with primers TOGFF1and TOGFR1 in the former case and primers TOGFF2 and TOGFR2 in the latter case (see Table S2 in the supplemental material). The PCR products were digested with NsiI and subcloned into pGEM-T Easy (Promega Corp.) to derive the 5′ and 3′ *TOS9* fusion product. The latter was cloned into the pBluescript vector (Stratagene, San Diego, CA) to derive pK22.1. The green fluorescent protein (GFP)-ORF-Ca*CAG1* 3′ fusion fragment, derived from pJ49.1 (T. Srikantha and D. R. Soll, unpublished data) was fused in frame to the 5′ end of the *TOS9* ORF. The plasmid vector containing the GFP ORF was a generous gift from J. Berman, University of Minnesota (11). The *GFP-CAG1* fragment was amplified by PCR with primers GFCFF1 and CAGR1 (see Table S2 in the supplemental material), digested with PstI and SphI, and, together with a DNA fragment containing the nourseothricin resistance gene Ca*SAT1*^{r} (36), ligated between the NsiI and SphI sites to derive the plasmid derivative pK40.1, which contained the transformation module for targeting at the *TOS9* locus. In-frame fusion was confirmed by sequencing, and the transformation module containing Ca*SAT1*^{r} was excised by XhoI digestion and used to transform strain WUM5A. Two clones, TOGF1 and TOGF4, were verified by sequencing and Southern analysis.

Tetracycline-controlled *TOS9*. The GFP ORF of pNIM1, a generous gift from J. Morschhäuser, University of Würzburg, was replaced with the *C. albicans* *TOS9* ORF, obtained by PCR with strain WO-1 genomic DNA and primers 4884Sal and 4884Bgl (see Table S2 in the supplemental material). The resulting plasmid, pJ83.1, was verified by sequencing. Plasmid DNA was digested with ApaI and SacII, and the expression cassette was used to transform strain WUM5A. Transformants Wr1 and Wr2 were verified by Southern analysis. Activation by doxycycline was demonstrated by Northern analysis of *TOS9*.

***MET3*-controlled *TOS9*.** To generate a *MET3*::*TOS9* expression module, 665 bp of the *MET3* promoter and 325 bp of the 3′-flanking region of the *MET3* ORF, respectively, were amplified by PCR from WO-1 genomic DNA. Primers mesmsaf1 and mepsnrr1 were used to derive the 5′-flanking region, and mepsbgf2 and mesmsar2 were used to derive the 3′-flanking region (see Table S2 in the supplemental material). The PCR products were digested with PstI and fused by ligation-mediated cloning into plasmid pGEM-T Easy to derive pK54.2. The *SAT*^{r} marker DNA derived by PCR with primers SATBglf1 and SATSphr1 (see Table S2 in the supplemental material) was digested with BglII and PstI and directionally ligated to BglII-PstI-digested pK54.2 to derive pK75.2. The *TOS9* ORF, derived by PCR with primers TOGSbF1 and TOSbsR1 (see Table S2 in the supplemental material), was digested with SbfI and ligated at the PstI site of pK75.2 to derive pK83.10. The orientation of the *TOS9* ORF was verified by sequencing. Plasmid DNA was digested with SacII and transformed into *TOS9* null mutant TOHO3. The transformants were analyzed for correct targeting at the *MET3* locus with primers METPCR and TO5r1 (see Table S2 in the supplemental material). Transformants Thomet3, Thomet4, Thomet6, and Thomet10 were selected for rescue analysis.

RACE (rapid amplification of cDNA ends) analysis. To determine the untranslated regions of the *TOS9* mRNA, total RNA from opaque WUM5A cells was analyzed by both 5′ RACE and 3′ RACE with the SMART RACE cDNA amplification kit (Clontech, Mountain View, CA) according to the manufacturer's specifications. For 5′ RACE products, the UPM primer supplied with the kit was used with either *TOS9*-specific primer TO5r1 or TO5r2, and for 3′ RACE products, the primer TOS9f4 was used (see Table S2 in the supplemental material). The PCR products were cloned into the pGEM-T Easy vector (Promega Corp.) and sequenced.

Temperature-induced mass conversion. Cells were grown in suspension to the late exponential phase of growth at 25°C in modified Lee's medium and then diluted three- to fourfold into fresh medium at 42°C (45). Cells were removed at time intervals (i) for cell density measurements with a hemocytometer; (ii) for assessment of the time of phenotype commitment by plating onto agar, incubation at 25°C for 7 days, and measurement of the proportions of white and opaque

colonies; and (iii) for assessment of *TOS9* and *OP4* expression by Northern analysis.

Visualization of GFP-Tos9p. GFP-labeled Tos9p fluorescence was visualized with the Bio-Rad Radiance 2000MP confocal microscope system on a Nikon TE2000U microscope equipped with the 60× Plan Apochromat water immersion objective (numerical aperture, 1.2) and a 4× digital zoom. LaserSharp 2000 (release 5.2) software was used for image acquisition and fluorescence quantitation. GFP was excited with the 488-nm argon laser line at 20% power and two-scan accumulation. The same acquisition parameters were used for all samples. 4′,6′-Diamidino-2-phenylindole (DAPI) staining was performed by the methods of Hazan and Liu (14).

Western analysis of Myc transformants. Cells were washed in Dulbecco's phosphate-buffered saline (Gibco Invitrogen, Grand Island, NY) containing a protease inhibitor cocktail (P8215; Sigma, St. Louis, MO) and 1 mM phenylmethylsulfonyl fluoride. Extracts were clarified by low-speed centrifugation, and protein concentrations were determined with Coomassie Plus protein assay reagent (Pierce, Rockford, IL). Western assays were run as previously described (15). The 9E10 anti-Myc antibody developed by J. M. Bishop was obtained from the Developmental Studies Hybridoma Bank (Iowa City, IA). The 9E10 supernatant was diluted 1:10 in TBS-T (20 mM Tris-HCl, pH 7.5, 150 mM NaCl, 0.05% Tween 20) and incubated with the membrane for 2 h at room temperature. The membrane was then washed four times in TBS-T. The primary antibody was detected with horseradish peroxidase-labeled goat anti-mouse immunoglobulin G (Promega, Madison, WI), diluted 1:10,000 in blocking buffer (3% nonfat dry milk in TBS-T), developed with SuperSignal West Pico Chemiluminescent Substrate (Pierce, Rockford, IL), and exposed to X-ray film (Eastman Kodak, Rochester, NY).

RESULTS

Generation of strains with Myc-tagged a1p or α2p for ChIP-chip analysis. Derivatives of a *C. albicans* **a**/α strain were generated that expressed Myc-tagged **a**1 or α2 for ChIP-chip analysis (Fig. 1A). Several derivatives of each were identified and verified by Southern blot analysis and sequencing. As was the case for the parent strain, neither of the two selected Myc-tagged derivatives, **a**1-29.1 or α2-3.1, formed opaque colonies or opaque sectors after 7 days of incubation at 25°C (Fig. 1B, C, and D). The frequencies of switching of the selected strains were estimated to be less than 10^{-6}, at least more than 3 orders of magnitude lower than that of **a**/**a** and α/α strains (4, 31, 37, 40, 42), indicating that the expressed Myc-tagged proteins functioned normally in the **a**1-α2 complex in repressing switching. Western blot analysis with anti-Myc antibody revealed similar levels of Myc-tagged **a**1 and α2 expression in the respective Myc-tagged derivatives (Fig. 1E). To demonstrate that Myc-tagged **a**1 and α2 bound correctly to target DNA sequences, chromatin immunoprecipitated with anti-Myc antibody was tested by PCR for enrichment of the *CAG1* promoter, since *CAG1* is repressed by the **a**1-α2 complex (17). Anti-Myc chromatin immunoprecipitates were enriched for the *CAG1* promoter sequence (Fig. 1F), demonstrating that the repressor complex containing either Myc-tagged **a**1 or Myc-tagged α2 bound to an expected target.

To map **a**1-α2 binding sites across the *C. albicans* genome, a high-density oligonucleotide-tiling array was designed that covered each sequence contig present in assembly 19 of the *C. albicans* genome (19) at an average resolution of 40 bp, for a total of 369,803 oligonucleotides, each 50 bp in length. ChIP was performed independently with epitope-tagged **a**1 and α2 strains (Fig. 2), and three biological replicates were performed for each factor. Following data acquisition, the mean signal for each oligonucleotide was calculated and used to plot the level of immunoprecipitation enrichment across each contig. Because of the nature of the oligonucleotide array, clear enrichment peaks were observed that included multiple oligonucleotides (Fig. 2).

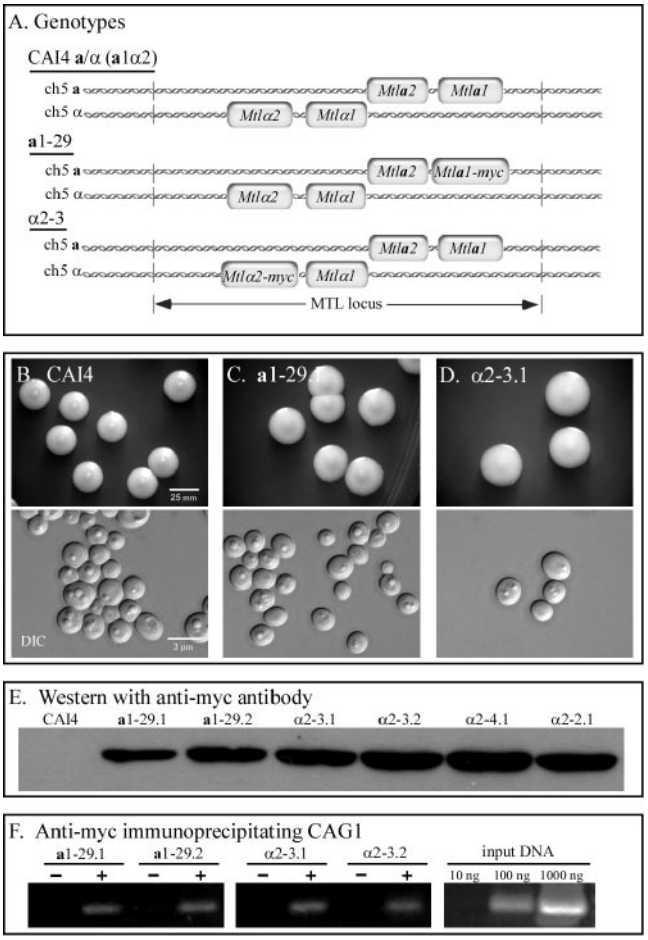

FIG. 1. The strains used for ChIP-chip analysis normally suppressed switching. (A) The genotype of the strains used to identify targets of the **a**1-α2 repressor complex. (B, C, and D) Cells from the parent CAI4 strain and the Myc-tagged **a**1 (**a**1-29) and α2 (α2-3) strains formed normal white colonies and cells with the round, white phenotype, indicating that tagged **a**1 and α2 fully retained repressor function. (E) Western blot treated with anti-Myc antibody. (F) ChIP with anti-Myc antibody and subsequent PCR of *CAG1*, a known target of the **a**1-α2 complex reveal specific Myc-tagged **a**1 and α2 binding. In panel F, a minus indicates the absence of anti-Myc antibody and a plus indicates the presence of anti-Myc antibody in the immunoprecipitation procedure. DIC, differential interference contrast.

To obtain a comprehensive list of the regions displaying enrichment, the array data were normalized and scored for the presence of statistically significantly enriched regions with Tilescope ($P > 1 \times 10^{-4}$, pseudomedian signal, ≥1.15; Zhang et al., submitted). The ORF immediately downstream of the binding peak was determined by using the human-curated *C. albicans* genome annotation (6) (Table 1). The peak binding site was determined from the $\log_2$ ratios of tagged versus untagged signal in a binding region (Fig. 2). Binding site locations were determined as the number of nucleotides (base pairs) upstream (−) or downstream (+) from the translation ATG initiation site (Table 1). The **a**1p and α2p binding sites ranged

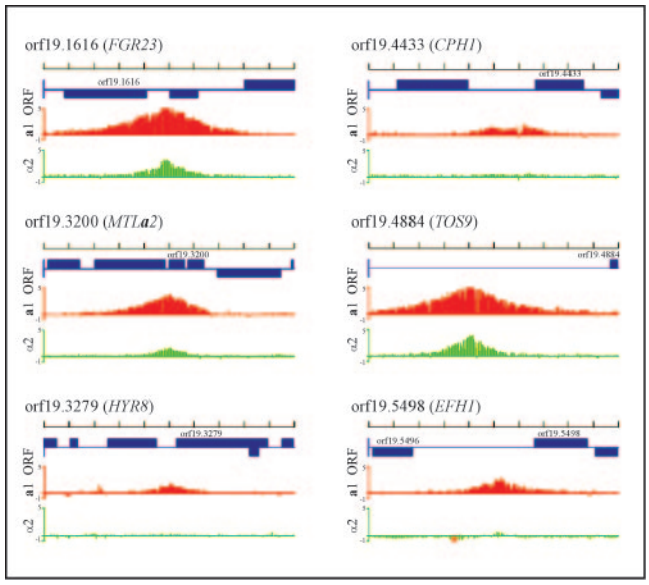

FIG. 2. *MTL***a**1 and *MTL*α2 bind to discrete genomic loci throughout the genome of *C. albicans*. Six examples of genomic regions enriched by the ChIP-chip procedure with **a**1 (red) or α2 (green). The $\log_2$ ratios of tagged versus untagged signals are presented for each factor below the locations of the predicted ORFs for the genomic region (dark blue) with the ORFs predicted to be regulated by the binding event indicated with their systematic names. The scale above each region represents 10 kb in 1-kb increments.

from −5,647 bp upstream from the translation initiation site to sites within an ORF (Table 1).

Genes identified by ChIP-chip analysis. ChIP-chip analysis of Myc-tagged **a**1 identified 52 target genes (Table 1). One-fourth of them had mating-related functions (*FGR23*, *CAG1*, *MFalpha*, *STE4*, *MTL***a**2, *SAP98*, *FAR1*, *STE18*, *CEK2*, *CPH1*, *ASF1*, *STE2*, and *TOS9*). In a previous microarray analysis, six of these genes (*CEK2*, *STE2*, *FAR1*, *FGR23*, *CAG1*, and *TOS9*) were found to be up-regulated in *MTL*-homozygous cells (49). Seven of the genes identified by **a**1p binding had deduced functions in development or morphogenesis (*YGR284C*, *FGR23*, *PGA55*, *MHP1*, *19.3851*, *HYR8*, and *IFI3*), six had deduced functions in the regulation of transcription (*MTL***a**2, *SAC3*, *EFH1*, *RXT3*, *CPH1*, and *ASF1*), four had deduced functions in the cell cycle and/or cytoskeleton (*FAR1*, *WHI3*, *MHP1*, and *SCP1*), one had a deduced function in drug resistance (*19.4883*), three had deduced functions in DNA replication or repair (*PSO2*, *REV3*, and *19.695*), five had deduced functions in transport (*TRS33*, *AVT7*, *AVT1*, *PTH2*, and *RHB1*), four had deduced functions in metabolism (*LEU6*, *ARH2*, *FRE3*, and *SNF3*), and three had deduced functions in membrane integrity or function (*19.1348*, *YBR147w*, and *19.1368*) (Table 1). Ten had no known function (Table 1). ChIP-chip analysis of Myc-tagged α2 identified 25 genes, all of which were also identified by Myc-tagged **a**1 analysis. For every target, the peak binding site for α2p was similar to that for **a**1p (Table 1).

Since it had been hypothesized that spontaneous switching in *MTL*-homozygous strains may be the result of position-effect variegation mediated by adjacent silencing regions (21, 41, 42, 46), the chromosome locations of **a**1 and α2 binding sites were mapped in relation to telomeres and centromeres. Six target genes (*ASF1*, *CPH1*, *19.1384*, *PTH2*, *STE18*, and *WH13*) were within 50 kb of centromeres, and two (*FAR1* and *PSO2*) were within 50 kb of telomeres (see Fig. S1 in the supplemental material).

Identification of candidate MSG and MSG activator genes. We hypothesized that phenotypic switching would involve a metastable switch between silent and expressed states of an MSG. In **a**/α cells, switching would be repressed by the **a**1-α2 corepressor complex at the MSG (Fig. 3A) or at a gene that encodes an activator of MSG metastability (Fig. 3B). Hence, in **a**/α cells, the MSG would be stably locked into one of the two states. In **a**/**a** and α/α cells, absence of the **a**1-α2 complex would lead to MSG metastability and, hence, switching (Fig. 3C and D). Northern analysis of genes with **a**1-α2 binding sites was therefore performed with **a**/α cells, white and opaque α/α cells, and white and opaque **a**/**a** cells. If a gene with an **a**1-α2 binding site was constitutively expressed in all cell types, it was tentatively excluded as a candidate MSG or MSG activator gene (Fig. 3E). If a gene with an **a**1-α2 binding site was silent in **a**/α cells but expressed in either **a**/**a** or α/α cells, it was tentatively excluded as a candidate MSG or MSG activator gene (Fig. 3E), since switching in both **a**/**a** and α/α cells is similarly released from **a**1-α2 repression (30, 31). If a gene was silent in **a**/α cells but expressed in either the opaque or the white type of both **a**/**a** and α/α cells, it was considered a candidate MSG (Fig. 3E). Finally, if a gene was silent in **a**/α cells but expressed in both white and opaque **a**/**a** and α/α cells, it was considered a candidate MSG activator gene (Fig. 3E) on the basis of the assumption that an activator would be essential for switching in both the white-to-opaque and opaque-to-white directions in both **a**/**a** and α/α cells (Fig. 3E). While other interpretations of patterns were plausible, the major ones depicted in Fig. 3E provided a contextual framework for initial screening.

Of the 52 genes analyzed, 25 provided analyzable Northern blot hybridization patterns. For the remaining 27 genes, there was either no Northern blot hybridization signal or a signal too weak or nondiscrete to analyze. Of the 25 genes with interpretable expression patterns, 15 were constitutively expressed (Fig. 3E and F; Table 1) and therefore excluded as candidates. One gene, *MTL***a**2, was **a** specific, a second, *SAP98*, was **a**/**a**-opaque specific, and a third, *MFalpha*, was α/α-opaque specific (Fig. 3C and D; Table 1). These genes were also excluded as candidates. Only one target gene, *TOS9*, exhibited an expression pattern consistent with a candidate MSG. *TOS9* was expressed in neither **a**/α cells nor white **a**/**a** and α/α cells; it was expressed in opaque **a**/**a** and opaque α/α cells (Fig. 3C and D; Table 1). *TOS9*, which has more recently been referred to as *EAP2* in *C. albicans* (27), has homologs in *Schizosaccharomyces pombe* (22) and *S. cerevisiae* (50, 51). These homologs, referred to in both strains as *TOS9*, have been implicated in mating, gluconate transport, endoplasmic reticulum (ER) regulation, budding, and cell adhesion.

Six genes, *STE4*, *STE18*, *PSO2*, *FAR1*, *CEK2*, and *CAG1*, exhibited expression patterns consistent with a candidate MSG activator gene. These genes were silent in **a**/α cells but expressed in both opaque and white **a**/**a** and α/α cells (Fig. 3C and D; Table 1). Since *CAG1*, *STE4*, and *STE18* are G-protein subunits involved in pheromone signal transduction, *CEK2* is a

TABLE 1. **a**1p and α2p binding target genes identified by ChIP-chip analysis

Gene	ORF	Contig	Chromosome	**a**1p peak signal	**a**1p binding peak[a] (bp)	α2p peak signal	α2p binding peak[a] (bp)	Deduced function	Expression pattern[b]
YGR284c	19.566	1524		2.828	+ (1,159)	2.828	+ (1,144)	Induced in a morphology-dependent manner	
FGR23	19.1616	10123	3	2.789	− (608)	1.582	− (758)	TUP1 controlled, induced in hypha and by pheromone	
CAG1	19.4015	10194	5	2.638	− (198)	1.563	− (168)	Alpha subunit of trimeric G-protein complex	Wh **a**, α; Op **a**, α (C.A.)
NA[c]	19.4883	10215	1	2.472	− (4,688)	1.989	− (4,703)	Unknown; resistance to antifungal ciclopirox olamine	Constitutive
TOS9	19.4884	10215	1	2.472	− (5,647)	1.989	− (5,632)	Unknown; has a pka1 phosphorylation motif (KRWTDG); mating role	Op **a**, α (C. MSG)
Mfalpha	19.4481	10206	1	2.3	− (416)	1.418	− (371)	Alpha pheromone gene	Op α
IFI3	19.4482	10206	1	2.3	− (1,300)	1.418	− (1,345)	Unknown; TAIP-2 apoptosis protein 2	Constitutive
STE4	19.799	10076	2	2.226	− (766)	1.248	− (961)	Beta subunit of trimeric G-protein complex	Wh **a**, α; Op **a**, α (C.A.)
NA	19.1384	10113	2	2.14	+ (644)	2.242	+ (732)	Unknown	
*MTL**a**2*	19.32	10170	5	2.124	− (142)	1.224	+ (38)	Transcription factor required for mating of **a**/**a** cells	Wh **a**; Op **a**
SAP98	19.852	10076	2	2.12	− (800)	2.414	− (755)	Glycosyl-phosphatidylinositol-anchored aspartic endopeptidase; only **a**/**a** cells	Op **a**
STE18	19.6551.1	10248	7	2.12	− (63)	1.165	− (18)	Gamma subunit of trimeric G-protein complex	Wh **a**, α; Op **a**, α (C.A.)
PSO2	19.5362	10225	2	2.038	+ (174)			DNA cross-link repair protein	Wh **a**, α; Op **a**, α (C.A.)
NA	19.1348	10111	2	1.828	+ (311)			Unknown; predicted membrane-spanning domain	
NA	19.1349	10111	2	1.828	− (1,339)			Unknown	
PGA55	19.207	10045	2	1.811	+ (1,548)			Unknown; regulated by Nrg1p and Tup1p	
DFG10	19.209	10045	2	1.811	− (3,451)	1.944	− (3,466)	Unknown; has a role in filamentous growth	
KIC1	19.191	10044	2	1.746	− (397)			Protein kinase of PAK/STE20 family, interacts with Cdc31p	Constitutive
FAR1	19.7105	10262	7	1.74	+ (22)			Cell cycle regulator, inhibits G1 cyclins, polar during mating	Wh **a**, α; Op **a**, α (C.A.)
WHI3	19.6494	10248	7	1.734	− (1,781)			RNA binding protein, cell cycle arrest through CLN3 mRNA	
TRS33	19.6496	10248	7	1.734	− (785)			Role in ER-to-Golgi transport, in transport protein particle	Constitutive
CEK2	19.46	10052	R	1.728	+ (122)			Mitogen-activated protein kinase, mating	Wh **a**, α; Op **a**, α (C.A.)
MHP1	19.461	10052	R	1.728	− (1,812)			Role in microtubule stabilization and filamentous growth	
NA	19.3851	10193	R	1.693	− (808)			Unknown; possibly regulatory in development	
LEU6	19.1375	10113	2	1.606	− (780)	1.548	− (765)	Leucine biosynthesis	
SAC3	19.1555	10119	2	1.583	+ (1,947)	1.829	+ (1,932)	Role in transcription and mRNA export	
YBR147w	19.1364	10113	2	1.542	− (859)	2.02	− (724)	Unknown; has membrane-spanning domain	Constitutive
Pa*IFZ2*	19.1365	10113	2	1.542	− (435)	2.02	− (570)	Unknown; similar to *Pseudomonas aeruginosa* protein AE004658	Constitutive
AVT1	19.5496	10228	2	1.536	− (3,394)			Gln (Asn), Ile (Leu), Tyr vacuolar transporter	
EFH1	19.5498	10228	2	1.536	− (1,482)			Transcription factor of basic helix-loop-helix family paralogous to EFG1	Constitutive
SCP1	19.17	10014	2	1.428	− (130)			Transgelin like; cross-links actin, binds actin	Constitutive
RXT3	19.3568	10183	2	1.391	− (1,305)	1.441	− (1,290)	Similar to Ybr112c/Cyc8; general repressor of transcription	
YLR407w	19.3569	10183	2	1.391	− (1,191)	1.441	− (1,266)	Unknown; localized to cell periphery as GFP fusion	Constitutive
NA	19.1368	10113	2	1.389	− (2,282)	1.353	− (2,147)	Unknown; possible outer membrane lipoprotein	
NA	19.1369	10113	2	1.389	− (2,632)	1.353	− (2,767)	Unknown; similar to *P. aeruginosa* protein AE004481	
AVT7	19.905	10076	2	1.356	− (1,238)	1.528	− (1,193)	Putative transporter of γ-aminobutyric acid–glycine	Constitutive
ROM2	19.906	10076	2	1.356	− (1,918)	1.528	− (2,323)	Rho guanyl nucleotide exchange factor activity	
RHB1	19.5994	10236	3	1.353	− (2,409)			GTPase activity, canavanine resistance, arginine uptake	
PTH2	19.4231	10202	5	1.331	− (570)			Mitochondrial peptidyl tRNA hydrolase; proline transport	Constitutive
CPH1	19.4433	10205	1	1.253	− (1,706)			Transcription factor; mating	Constitutive
NA	19.439	10203	R	1.242	− (1,250)			Possible role like SW2/SNF transactivator complex	
HYR8	19.3279	10172	R	1.237	− (178)			Unknown; glycosyl-phosphatidylinositol anchored, hypha regulated	Constitutive
CPH1	19.4433	10205	1	1.221	− (206)			Transcription factor; mating	Constitutive
ARH2	19.3521	10183	2	1.207	− (1,085)	1.506, (1.486)	− (785), − (1,280)	Adrenodoxin-NADPH oxidoreductase; role in heme biosynthesis	
REV3	19.3522	10183	2	1.207	− (1,252)	1.506, (1.486)	− (1,552), − (1,057)	Zeta DNA polymerase activity, reverse transcriptase, DNA repair	
ASF1	19.3715	10188	R	1.195	− (239)			Anti-silencing protein; affects silent mating locus	
NA	19.3716	10188	R	1.195	− (2,624)			Unknown; transcription divergent to ASF1	
FRE8	19.701	10065	R	1.174	− (2,359)			Similar to ferric reductase, flucytosine repressed, adherence induced	
NA	19.446	10052	1	1.143	− (580)			Unknown; Zn^{2+} finger, transposase domain	Constitutive
NA	19.695	10065	R	1.104	− (8,049)			Activated by GTPase, suppressor of POLI/POLIII mutant AC40	
STE2	19.696	10065	R	1.104	− (278)			Mating pheromone alpha receptor	
SNF3	19.5962	10236	3	1.038	− (882)			Glucose sensor; induced by macrophages, down in biofilm	Constitutive
NA	19.5963	10236	3	1.038	− (291)			Unknown; possibly located in membrane, ER	

[a] +, downstream of start codon, ATG; −, upstream of start codon, ATG.
[b] Wh, white; Op, opaque; C.A., expressed in both white and opaque, candidate MSG activator; C. MSG, candidate master switch gene (see Fig. 3 for details).
[c] NA, not applicable.

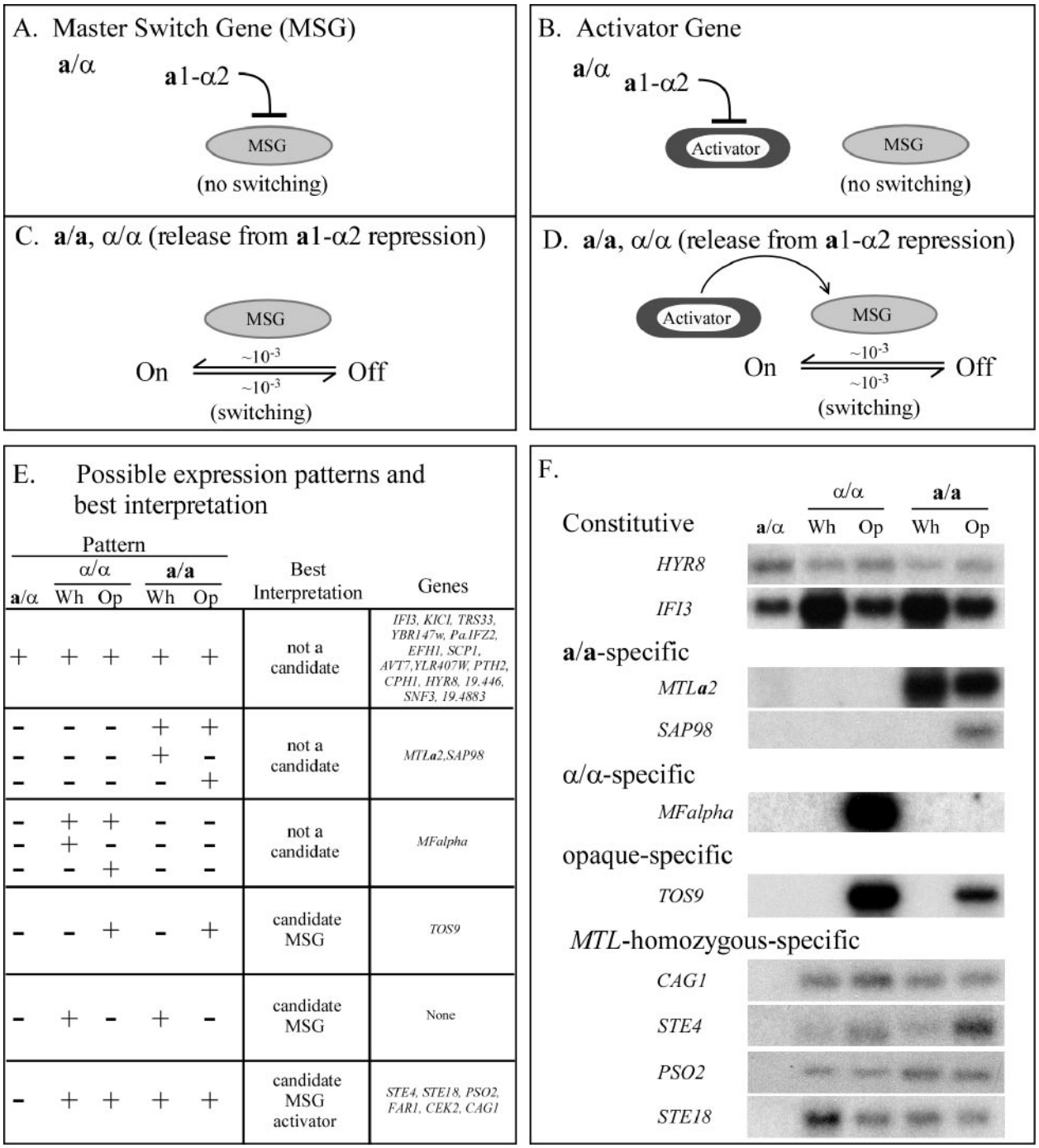

FIG. 3. Transcription profiles were used to identify candidate MSGs and candidate activators of MSGs. (A) Model of **a**1-α2 repression of MSG expression in **a**/α cells. (B) Model of **a**1-α2 repression of an MSG activator. (C) MSG activation of switching in **a**/**a** or α/α cells. (D) Role of an MSG activator in switching. (E) Possible expression patterns, best interpretations of expression patterns, and genes that fit the patterns in the different categories. (F) Examples of gene expression patterns revealed by Northern analysis in the different categories. Wh, white; Op, opaque.

mitogen-activated protein kinase involved in the pheromone signal transduction pathway and *FAR1* is a regulator of pheromone-induced G_1 arrest and cell polarization, they were considered unlikely MSG activator gene candidates. This left *PSO2* as the only possible MSG activator candidate. *PSO2* encoded a protein with a deduced function in DNA cross-linking and repair and was located within 15 kb of a telomere on chromosome 2 (see Figure S1 in the supplemental material).

Tos9p localizes in the nucleus. Although *TOS9* was a candidate MSG on the basis of its expression pattern (Fig. 3), it was not located close to either a centromere or a telomere along chromosome 1 (see Figure S1 in the supplemental material). The *TOS9* ORF encoded a putative protein of 785

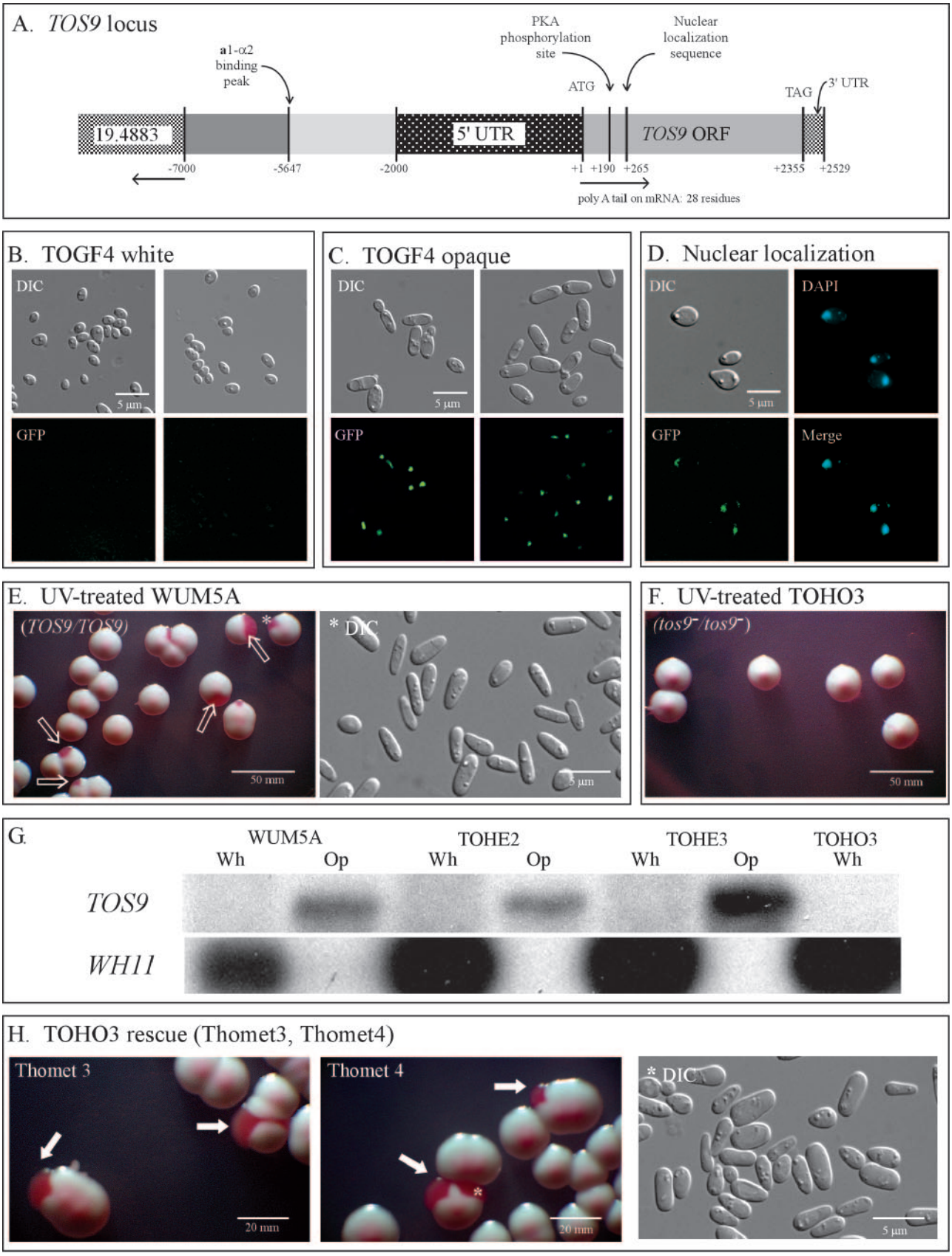

FIG. 4. Deletion of *TOS9* results in cells that cannot switch and are blocked in the white phase. (A) Description of *TOS9* and its 5′ upstream region. The transcription start and stop sites and poly(A) tail were identified by RACE analysis. The directions of transcription of *TOS9* and the

amino acids. A 7,000-bp region upstream of *TOS9* was devoid of an ORF (Fig. 4A). The peaks for **a**1p and α2p binding in this region were 5,647 and 5,632 bp, respectively, upstream of the ORF (Table 1). 5′ and 3′ RACE analyses revealed a transcription start site 2,000 bp upstream of the ATG start codon and a transcription termination site 174 bp downstream of the TAG stop codon (Fig. 4A), indicating a transcript size of approximately 4.5 kb. 3′ RACE analysis also revealed a relatively short poly(A) tail of 28 residues. Divergently transcribed ORF 19.4883, of unknown function, was approximately 7,000 bp upstream from the *TOS9* ORF and 1,850 bp upstream of the **a**1-α2 binding region (Fig. 4A). This gene, however, was constitutively expressed (Table 1) and therefore excluded as a candidate MSG or activator of an MSG. The deduced Tos9 protein contained a putative protein kinase A binding site (KRWTDG) between +190 and +208 bp and a putative bipartite nuclear localization sequence (KKNLIDKDKKKKKK AKFG) between +265 and +318 bp (Fig. 4A).

Since the deduced *TOS9* protein contained a nuclear localization sequence, we replaced one copy of *TOS9* in strain WUM5A, a *ura3*$^-$ derivative of strain WO-1 (47), with a *TOS9* ORF fused in frame with *GFP* at the carboxy terminus, to generate strain TOGF4. This strain was used to examine the subcellular localization of Tos9p by laser scanning confocal microscopy. White cells of strain TOGF4 exhibited no fluorescent signal (Fig. 4B), whereas opaque cells exhibited a strong fluorescent signal that localized exclusively in the nucleus (Fig. 4C and D).

***TOS9* null mutants do not switch.** To test whether *TOS9* plays a role in switching, a *TOS9* null mutant was generated with the recyclable SAT^r cassette and the maltose-inducible flipper in strain WUM5A (36, 47). Three heterozygous deletion derivatives, TOHE1, TOHE2, and TOHE3, were generated. The homozygous deletion derivative TOHO3 was then generated from TOHE3. Deletions were verified by Southern analysis and sequencing. When cells from 4-day-old white colonies of strain WUM5A were plated on nutrient agar at 25°C, they formed white colonies with opaque sectors at a frequency of 10^{-2} to 10^{-3} after 8 days. When cells from 4-day-old white colonies of strain TOHE2 were similarly plated, they formed opaque sectors after 8 days but at a lower frequency than WUM5A. When cells from 4-day-old colonies of strain TOHE3 were similarly plated, no sectors were observed. However, TOHE3 formed opaque sectors when treated with low doses of UV irradiation (data not shown), a treatment previously demonstrated to stimulate white-opaque switching in wild-type cells (32). Cells from the opaque sectors of *TOS9* heterozygous deletion mutants exhibited the typical opaque phenotype.

Colonies of the *TOS9* homozygous deletion mutant TOHO3 did not produce opaque sectors, even after 14 days at 25°C. Treatment with low doses of UV irradiation, which induced switching to the opaque phase in parallel cultures of parent strain WUM5A (Fig. 4E), did not induce switching in TOHO3 (Fig. 4F). Northern analysis revealed that *TOS9* was selectively

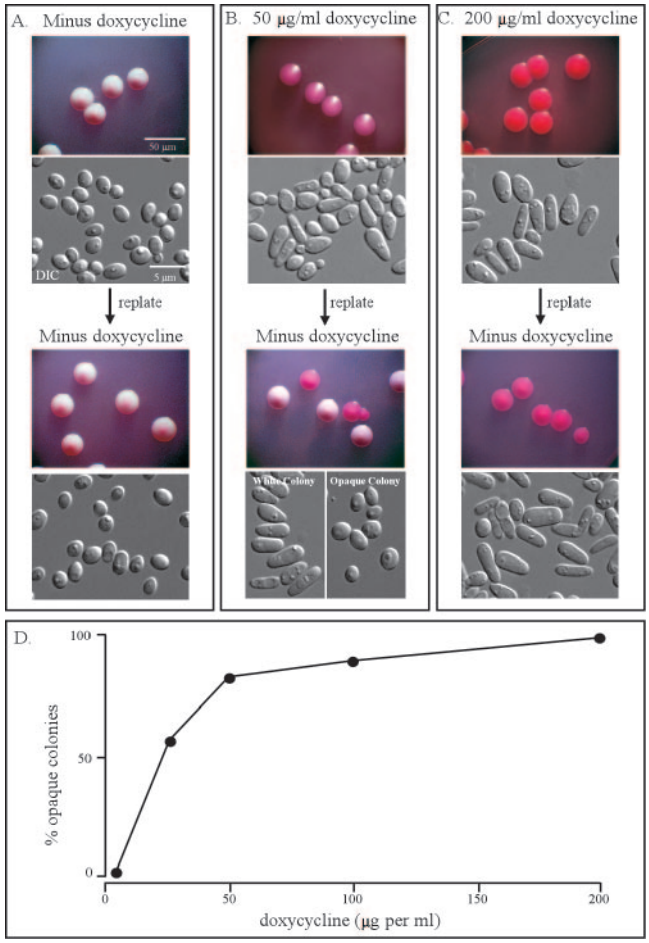

FIG. 5. Misexpression of *TOS9* in white cells causes mass conversion to the opaque phase. *TOS9* was placed under the control of a tetracycline (doxycycline)-inducible promoter at an ectopic site in *TOS9*/*TOS9* parent strain WUM5A to generate strain Wr1. (A, B, C) White, pink, and red colonies of Wr1 cells treated with 0, 50, and 200 μg/ml doxycycline, respectively, contained white, white plus opaque, and opaque cells, respectively. Replating in the absence of doxycycline demonstrated white, a mixture of white and opaque, and opaque colonies, respectively. (D) Dose-response curve of doxycycline induction of the switch from white to opaque in strain Wr1. Data from two experiments, each including 200 colonies per doxycycline concentration, were pooled. The data from the two were highly similar.

divergently transcribed gene 19.4883 are denoted by straight arrows. (B) Differential interference contrast and fluorescence images of white cells of strain TOGF4 which express *TOS9* tagged at its carboxy terminus with GFP. (C) Differential interference contrast and fluorescence images of opaque cells of stain TOGF4. (D) Costaining of DAPI and GFP in TOGF4 demonstrates that Tos9p is localized to the nuclei of opaque cells. (E, F) UV treatment of parent strain WUM5A and the *TOS9* null mutant TOHO3 stimulated switching only in the former. (G) *TOS9* is transcribed selectively in opaque cells of WUM5A and heterozygous mutants TOHE2 and TOHE3. It is not expressed in TOHO3 cells, which are blocked in white. Wh, white; Op, opaque. (H) The *TOS9* null mutant rescued by transformation with the *TOS9* ORF under the regulation of the *MET3* promoter formed opaque sectors in the absence of methionine and cysteine. DIC, differential interference contrast.

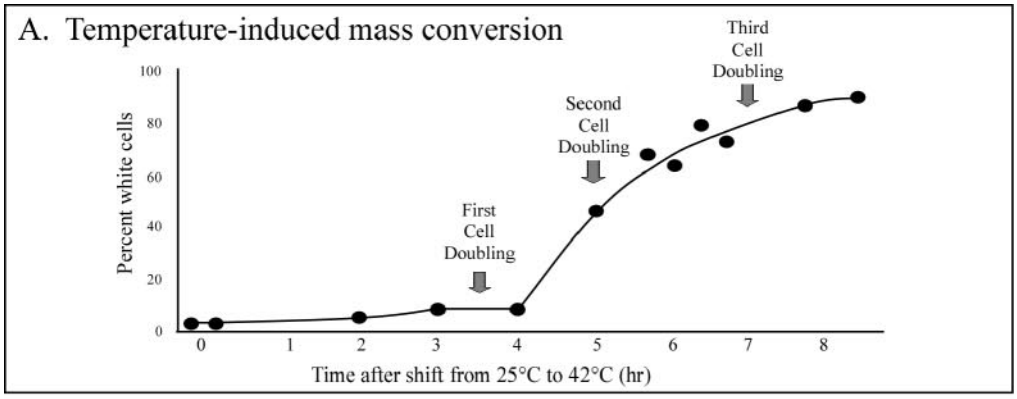

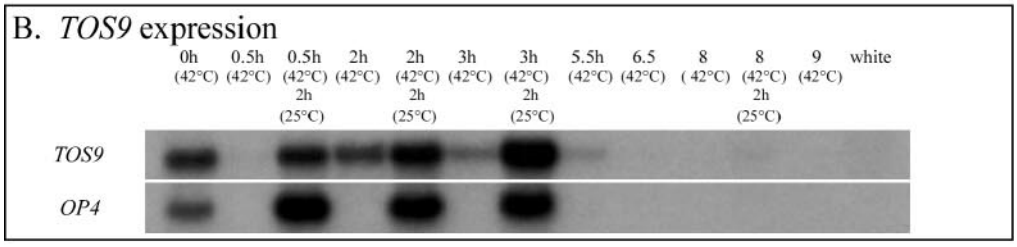

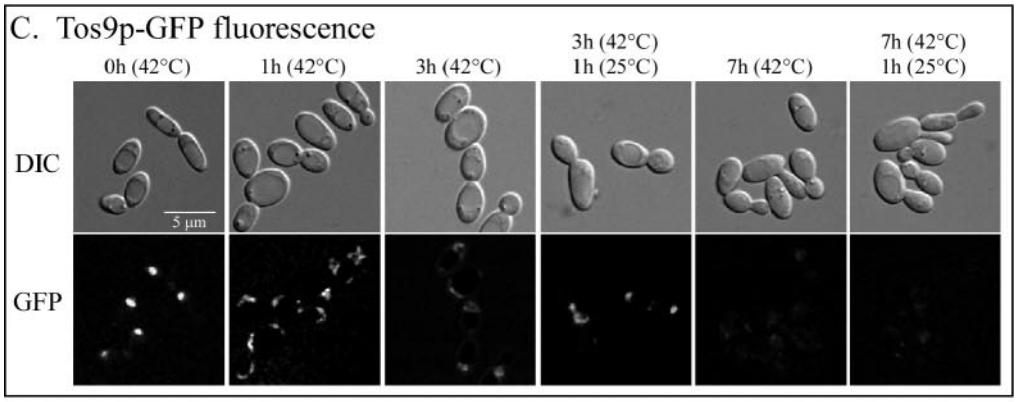

D. *TOS9* mixexpression inhibits temperature induced OP→Wh switch

Strain	Ectopic *TET*-TOS9	Temperature	Doxycycline	% opaque (7 hr)	% white (7 hr)
WUM5A	-	42°C	-	6	94
WUM5A	-	42°C	+	8	92
WUM5A	-	25°C	-	91	9
WUM5A	-	25°C	+	90	10
Wr1	+	42°C	-	13	87
Wr1	**+**	**42°C**	**+**	**93**	**7**
Wr1	+	25°C	-	85	15
Wr1	+	25°C	+	95	5

E. Hydroxyurea treatment

	Time $CH_4N_2O_2$ addition	Percent survival	Percent Op→wh 7h, 42°C
1.	——	100%	73%
2.	1.5h	75%	4%
3.	3.0h	74%	11%
4.	6.0h	93%	69%

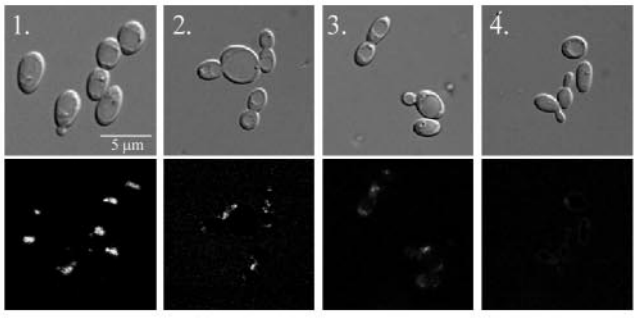

transcribed in the opaque phase of WUM5A, TOHE2, and TOHE3 but not in TOHO3 (Fig. 4G), which appeared to be blocked in the white phase. This latter conclusion was supported by the observations, first, that *WH11*, a white phase-specific gene, was selectively expressed in TOHO3 (Fig. 4G) and, second, that **a**-pheromone, which induces cohesiveness in white but not opaque α/α cells, a first step in biofilm formation (9), induced cohesiveness between TOHO3 cells (data not shown).

Heterozygous and homozygous deletion mutants of the candidate MSG activator *PSO2* were generated by the same strategy used to generate the corresponding mutants in *TOS9*. They were also similarly verified. Cells of the *PSO2* heterozygous mutant and null mutant switched to the opaque phase at the same frequency as parent strain WUM5A (data not shown). For that reason, *PSO2* was excluded as a candidate MSG activator gene.

Misexpression of *TOS9* in white a/a cells (*TOS9*/*TOS9*) causes mass conversion to the opaque state. The phenotype of the null mutant TOHO3 indicated that *TOS9* expression was essential for a switch from white to opaque. If *TOS9* played a role in the actual switching event, then misexpression in a white cell should drive the phenotype to opaque. To test this possibility, strain WUM5A (*TOS9*/*TOS9*) was transformed with a construct in which the *TOS9* ORF was under the regulation of a tetracycline (doxycycline)-inducible promoter (34), generating strain Wr1. The doxycycline-regulated construct was targeted ectopically to one of the two *ADH1* alleles (33). A control strain, Wnm1, was generated in which the *GFP* rather than the *TOS9* ORF was placed under the regulation of the doxycycline promoter. White Wr1 cells plated on nutrient agar lacking doxycycline formed predominantly (>99%) white colonies (Fig. 5A), which produced opaque sectors after 8 days at a frequency of 10^{-2} to 10^{-3}, similar to that of parent strain WUM5A. In contrast, white Wr1 cells plated on nutrient agar containing doxycycline at 50 μg/ml, the concentration used in previous studies to activate this promoter (34), formed almost exclusively (>99%) pink colonies (Fig. 5B). The proportion of opaque and white cells in these pink colonies varied between 50:50 and 80:20 (Fig. 5B). When cells from these pink colonies were replated on agar lacking doxycycline, the resulting colonies exhibited both the opaque and the white phenotypes (Fig. 5B). The red colonies contained almost predominantly opaque cells, and the white colonies contained predominantly white cells (Fig. 5B). When cells from pink colonies were replated on agar containing 50 μg/ml doxycycline, they formed both red and pink colonies (data not shown). The red colonies contained almost exclusively opaque cells, and the pink colonies contained a mixture of opaque and white cells (data not shown). An experiment in which the concentration of doxycycline was varied revealed that while 80 μg/ml induced switching in 80% of a white cell population, 200 μg/ml induced nearly all cells (>95%) to switch to the opaque state (Fig. 5D). Control Wnm1 cells behaved like parent cells. These results demonstrated that misexpression of *TOS9* in white *MTL*-homozygous cells induced mass conversion to the opaque state in a dose-dependent fashion, indicating that *TOS9* plays a role in inducing the switch from white to opaque.

Rescue of the *TOS9* null mutant. When the homozygous *TOS9* deletion mutant TOHO3 was transformed with the same doxycycline-inducible construct targeted to the same ectopic gene to generate strain To3r1 and the derived strain was plated on agar containing 200 μg/ml doxycycline, switching from white to opaque was not induced (i.e., there was no rescue of the mutant phenotype). This result suggested that an intact *TOS9* locus, with the native region upstream of the *TOS9* ORF, might be necessary for ectopic *TOS9* induction of a white-to-opaque switch. Northern analysis, however, revealed that the level of the *TOS9* transcript in doxycycline-treated To3r1 white cells was low, leading to an alternative explanation. Doxycycline induction of the ectopic *TOS9* ORF may be strong enough to initiate expression of the native *TOS9* gene, which in turn self-induces transcription to a level that drives a switch from white to opaque but alone may be too weak in TOHO3 to drive a switch. To distinguish between these alternative explanations, a transformation construct was generated in which the *TOS9* ORF was placed under control of the methionine-regulated promoter (7), which was potentially stronger than the tetracycline-regulated promoter. This construct was targeted to a *MET3* allele in TOHO3, generating the six rescued strains Thomet1 through Thomet6. Exclusion of both methionine and cysteine, which derepresses the *MET3* promoter, resulted in switching from white to opaque in tested rescue strains (Fig. 4H). The *TOS9* genotype of the opaque cells formed by the rescued strains was verified by PCR methods (data not shown). This result demonstrated that the phenotype of TOHO3 was due to deletion of the two *TOS9* alleles and that expression of *TOS9* in the absence of an intact *TOS9* locus can drive a switch from white to opaque.

Temperature-induced mass conversion and *TOS9* expression. Given that an increase in *TOS9* expression initiates and drives a switch from white to opaque, we expected that a decrease in *TOS9* expression would initiate and drive the reverse switch from opaque to white. To test this prediction, we

FIG. 6. When opaque cells were induced to mass convert to white by a shift from 25°C to 42°C, the *TOS9* transcript and protein levels decreased during the period preceding phenotypic commitment (the switch) to the white phenotype. The switch event was inhibited by addition of hydroxyurea just prior to the commitment event. It was also inhibited by misexpression of *TOS9* after the temperature shift. (A) The kinetics of phenotypic commitment to the white phase after an opaque cell population is shifted from 25°C to 42°C. The majority of cells commit to the white phase in concert with the second cell doubling. (B) The *TOS9* transcript level decreases to a negligible level after 0.5 h at 42°C, rebounds at 2 h, and then decreases to a very low level by 5.5 h. Reexpression to the original level before the temperature shift can be induced by reducing the temperature from 42°C to 25°C up to the point of phenotypic commitment to the white phase (1 h, 3 h) but not after phenotypic commitment (7 h). (C) Tos9p fluorescence decreases during the period preceding phenotypic commitment in strain Wr1. A reduction in temperature at 3 h, but not at 7 h, reestablishes Tos9p fluorescence in the nucleus. (D) Misexpression of *TOS9* at 42°C, by doxycycline induction of strain Wr1, blocks the temperature-induced switch to white (data in bold print). (E) Addition of hydroxyurea at 3 h, but not at 6 h, blocks commitment (the switch) to the white phase. Wh, white; Op, opaque.

first measured *TOS9* expression when parent WUM5A opaque cells were induced to undergo mass conversion to white by increasing the temperature from 25°C to 42°C (37, 40, 45). To monitor the point of commitment to the white phenotype at 42°C, cells were replated on nutrient agar at time intervals and incubated at 25°C and the phenotype of colonies was assessed after 4 days. The time period at 42°C after which a return to 25°C resulted in white rather than opaque colony formation was considered the point of commitment to the white phenotype. Cells in the population began committing to the white phenotype after 4 h, reaching 70% after 6.5 h, concomitant with the kinetics of the second cell doubling (Fig. 6A), as previously reported (42, 45). The *TOS9* transcript decreased to a negligible level within 30 min after cells were shifted from 25°C to 42°C, partially rebounded at 2 h, and then gradually decreased to a low level by 5.5 h (Fig. 6B). When cells were then returned from 42°C to 25°C prior to the commitment point (0.5, 2, and 3 h) and incubated for 2 h at 25°C, the *TOS9* transcript level was reestablished, but when they were shifted after the point of phenotypic commitment, the level was not reestablished (Fig. 6B). This pattern was similar but not identical to that of *OP4* (Fig. 6B), an opaque-specific gene, which decreased to a negligible level 0.5 h after the initial shift from 24°C to 42°C and remained negligible at the higher temperature (Fig. 6B). As was the case for *TOS9*, a shift back to 25°C prior to, but not after, phenotypic commitment reestablished the *OP4* transcript level (Fig. 6B).

To examine the fate of Tos9p, mass conversion was induced in an opaque-cell population that expressed GFP-tagged Tos9p (TOGF4) and at time intervals cell samples were examined by laser scanning confocal microscopy for GFP localization. Within 1 h after the temperature of an opaque cell culture was raised from 25°C to 42°C, Tos9p staining became more diffuse (Fig. 6C). After 3 h at 42°C, fluorescence was significantly reduced. If opaque cells were shifted from 42°C to 25°C at 3 h and incubated at the lower temperature for 1 h, fluorescence was reestablished in the nucleus (Fig. 6C). By 7 h, GFP fluorescence was undetectable and if these cells were returned to 25°C, fluorescence remained undetectable. (Fig. 6C).

To test whether the decrease in Tos9p is essential for temperature-induced mass conversion, *TOS9* was misexpressed after opaque cells were shifted from 25°C to 42°C. Strain Wr1 was used, which harbors, in addition to *TOS9* at the native locus, an ectopic copy of *TOS9* under control of the doxycycline-inducible promoter. In the absence of doxycycline, Wr1 underwent mass conversion, but in the presence of doxycycline, mass conversion was inhibited (Fig. 6D, inhibition data in bold print). These results demonstrated that the transition from opaque to white required down-regulation of *TOS9*.

Since commitment to the white phase (i.e., the switch from opaque to white) depended on a decrease in Tos9p, which occurred prior to the second cell doubling (42, 45), the possibility existed that the decrease in Tos9p and DNA replication, which preceded the second cell doubling, were both essential for the switch to occur. We therefore tested whether hydroxyurea, an inhibitor of DNA replication (13, 39), added just prior to the second cell doubling, inhibited the commitment event. Addition prior to commitment (0.5, 2, and 3 h) inhibited it (Fig. 6E). Cells inhibited by hydroxyurea still exhibited the same low level of Tos9p. These results demonstrated that a decrease in Tos9p was not sufficient for a switch to proceed. Cells still had to undergo DNA replication.

DISCUSSION

ChIP-chip analysis revealed 52 targets of **a**1-α2 binding in an **a**/α cell. Thirteen of these genes had known or deduced mating-related functions. A prior microarray analysis of transcription had demonstrated that 6 of these 13 genes were repressed in **a**/α cells and expressed in *MTL*-homozygous cells (49). Of the 52 targets of the **a**1-α2 corepressor, 25 provided distinct Northern blot hybridization patterns, and of these latter genes, only 1, *TOS9*, fit the predicted expression profile of an MSG while 6 fit the predicted expression pattern of an MSG activator. Of this latter group, five encoded proteins with specific functions in the pheromone transduction pathway and therefore were tentatively excluded as candidates, leaving only one candidate, *PSO2*. Mutant analysis demonstrated that while *TOS9* was essential for switching, *PSO2* was not. *TOS9* encoded a putative protein of 785 amino acids of unknown function. Recently, this gene was identified in a screen for *C. albicans* genes that promote adhesion and pseudohypha formation in an *S. cerevisiae flo8*Δ mutant deficient in these characteristics (27). They referred to the gene as *EAP2* for its capacity to stimulate adhesion of the *flo8*Δ mutant to epithelium. The *TOS9* homolog in *S. pombe* regulates mating in a cyclic-AMP-independent fashion (22) and is an inducer of gluconate transport (8). The homolog in *S. cerevisiae* has been implicated in regulation of the smooth ER (50), budding (51), and cell adhesion (27). *TOS9* was one of the six genes that had previously been identified by microarray analysis to be repressed in **a**/α cells and expressed in opaque **a**/**a** cells (49). By Northern analysis, we confirmed that *TOS9* was silent in **a**/α cells and transcribed exclusively in opaque cells, and not in white cells, of *MTL*-homozygous strains of *C. albicans*. By tagging Tos9p with GFP, we found that the protein was expressed only in opaque cells and localized to the nucleus, suggesting that it plays a role in gene regulation and/or DNA replication. The *TOS9* locus is unusual. The *TOS9* ORF is preceded by a 7,000-kb noncoding region. The **a**1-α2 binding site was approximately 5,647 bp upstream of the *TOS9* ORF (Fig. 4A). The binding site was also upstream of a divergently transcribed ORF, 19.4883, of unknown function. Since this latter gene was constitutively expressed, it was excluded as a candidate MSG or MSG activator. RACE analysis revealed that the transcription start site of *TOS9* was approximately 2,000 bp upstream of the ORF and 3,647 bp downstream of the **a**1-α2 binding site. It contained no intron. The estimated size of the *TOS9* transcript was therefore 4.5 kb. We found that expression of an ectopic copy of the *TOS9* ORF which lacked the extensive upstream region drove switching in the white-to-opaque direction under regulation of a tetracycline-induced promoter and blocked switching in the opaque-to-white direction under the regulation of the same promoter. Therefore, the 5′ untranslated region of the *TOS9* mRNA was not essential for *TOS9* induction of the white-to-opaque switch or inhibition of the opaque-to-white switch. It may, however, play a role during spontaneous switching in the regulation of mRNA half-life, a possibility now under analysis. The *TOS9* ORF con-

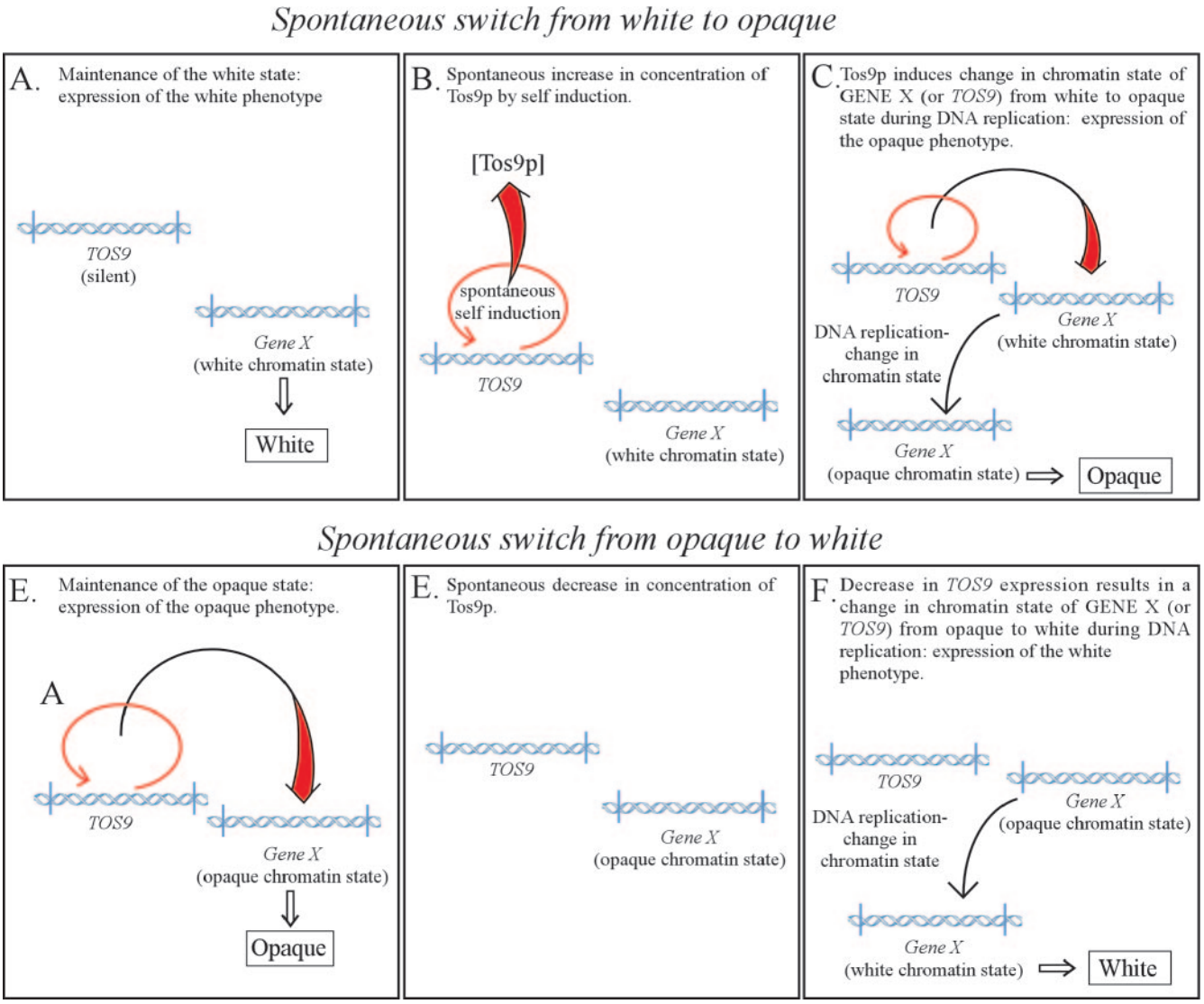

FIG. 7. A model for spontaneous switching between the white and opaque phases. The salient features of the model are the following. Spontaneous self-induction of *TOS9* expression in white leads to a change in chromatin state of an as-yet-unidentified switching locus, gene X. This change requires DNA replication. Continued expression of *TOS9* maintains the opaque chromatin state and hence the opaque phenotype. A spontaneous decrease in *TOS9* expression below a threshold results in a change in gene X from an opaque to a white chromatin state and, hence, a change to the white phenotype. The change in chromatin state of gene X activates its expression, but it is not clear if activation is in the white or the opaque state. Gene X must then regulate the pattern of phase-specific gene expression and phenotype. *TOS9* has not been excluded as the site of change. The correlation of commitment and the second cell doubling in the opaque-to-white transition suggests that opaqueness is the recessive state and whiteness is the dominant state, as previously proposed (41).

tained a putative protein kinase A binding site, suggesting that Tos9p may be regulated by phosphorylation. It also contained a nuclear localization signal, which was most probably responsible for nuclear localization.

Deletion of one of the two *TOS9* alleles did not block spontaneous switching to the opaque phenotype, but it did decrease the switching frequency, suggesting that the *TOS9* transcript level, and therefore the level of Tos9p, regulated the frequency of spontaneous switching. Deletion of both *TOS9* alleles resulted in the loss of switching and a block in the white phenotype. UV treatment, which stimulates switching by at least 2 orders of magnitude in wild-type cells (32), did not stimulate switching from white to opaque in the *TOS9* null mutant, indicating that *TOS9* was essential for the white-to-opaque transition. Furthermore, misexpression of ectopic *TOS9* in white cells with an intact *TOS9* locus caused mass conversion of the cell population to opaque. Resultant opaque cells were stable in the absence of doxycycline induction. This suggested that once stimulated in the white phase by misexpression of ectopically expressed *TOS9* (self-induction), the native *TOS9* gene continued to be expressed and, through this expression, maintained the opaque phenotype. When cells of the *TOS9* null mutant were transformed with the same doxycycline-inducible *TOS9* construct at the same ectopic locus and induced with doxycycline, they did not switch to the opaque phase, suggesting that the native locus was required. However, when

cells of the *TOS9* null mutant were transformed with a construct in which the *TOS9* ORF was under the regulation of the apparently stronger *MET3*-repressible promoter, they stably switched to the opaque state.

We have also demonstrated that during temperature-induced mass conversion from opaque to white, the *TOS9* transcript and protein decrease to low levels prior to phenotypic commitment. Misexpression of the *TOS9* ORF under control of the tetracycline-inducible promoter at an ectopic locus after an increase in temperature blocked the switch from opaque to white, suggesting that the level of Tos9p must decrease below a threshold for the switch from opaque to white to be initiated. The commitment event of an opaque-to-white switch, however, occurred at the time of second cell doubling following the increase in temperature (45) and presumably follows a second round of DNA replication (42). Inhibition of the second round of DNA replication with hydroxyurea, like misexpression of *TOS9*, blocked the temperature-induced switch to white without reestablishing Tos9p levels. This suggests that a switch requires two events, first, a decrease in the level of Tos9p and, second, DNA replication.

These results suggest a working model for spontaneous switching in which *TOS9* plays a central role. Based upon the effects on switching frequency of the histone deacetylase inhibitor trichostatin A and deletion of the histone deacetylases *HDA2* and *RPD3* (21, 46) and upon the dependency of the opaque-to-white switch on the second round of DNA replication demonstrated here, we hypothesize that stable switching events in both the white-to-opaque and opaque-to-white directions involve a change at a switch locus between the white and opaque chromatin states. We further hypothesize, on the basis of the functional analysis of *TOS9* presented here, that Tos9p directly or indirectly causes this change in chromatin state. The site of this change has not been established and has therefore been referred to in the model as gene X. While there is reason to believe that *TOS9* may not be the site of a *TOS9*-induced change in chromatin state, including the observations that it is self-inductive and can effect a switch through misexpression at an ectopic locus in the absence of the entire upstream region, including the large untranscribed region, it cannot be excluded. The product of gene X would be differentially expressed in the two switch phases and would regulate the patterns of phase-specific gene expression and, hence, phenotype (Fig. 7).

We hypothesize that a spontaneous switch from white to opaque at 25°C would be the result of a rare and stochastic increase in the level of Tos9p, which would self-stimulate further *TOS9* expression (Fig. 7B). Upon reaching a threshold level, Tos9p would induce a change from a white to an opaque chromatin state in gene X. This change would require DNA replication (Fig. 7C). The activation or repression of gene X effected by the change in chromatin state would lead to the opaque gene expression pattern and, hence, the opaque phenotype (Fig. 7D). The continued expression of *TOS9* above the threshold level by autostimulation would maintain the opaque state by directing continued gene X replication in the opaque chromatin state (Fig. 7D). We hypothesize that a spontaneous switch from opaque to white would involve a stochastic reduction in Tos9p below the threshold level (Fig. 7E). This would induce a change in chromatin state at gene X from the opaque to the white state, leading to a switch from the opaque to the white gene expression pattern and, hence, a change in phenotype (Fig. 7F). The change from the opaque to the white chromatin state would also require DNA replication. Because temperature-induced mass conversion of opaque cells to the white phenotype requires two rounds of DNA replication prior to phenotypic commitment, we previously proposed that the opaque chromatin state would be recessive and the white chromatin state would be dominant (42). Hence, while a switch from opaque to white should require at least two rounds of DNA replication, a change from white to opaque should require only one round. The validity of this working hypothesis is now being tested.

ACKNOWLEDGMENTS

We thank J. Collins for assembling the manuscript, Judith Berman of the University of Minnesota for pGFP plasmids, and Joachim Morschhäuser for strains and plasmids.

This research was supported by NIH grants AI2392 to D.R.S. and RO1-CA077808-9-13 to M.S.

REFERENCES

1. **Anderson, J. M., and D. R. Soll.** 1987. Unique phenotype of opaque cells in the white-opaque transition of *Candida albicans*. J. Bacteriol. **169:**5579–5588.
2. **Bedell, G., and D. R. Soll.** 1979. The effects of low concentrations of zinc on the growth and dimorphism of *Candida albicans*: evidence for zinc-resistant and zinc-sensitive pathways for mycelium formation. Infect. Immun. **26:**348–354.
3. **Bennett, R. J., and A. D. Johnson.** 2005. Mating in *Candida albicans* and the search for a sexual cycle. Annu. Rev. Microbiol. **59:**233–255.
4. **Bergen, M., E. Voss, and D. R. Soll.** 1990. Switching at the cellular level in the white-opaque transition of *Candida albicans*. J. Gen. Microbiol. **136:**1925–1936.
5. **Borneman, A. R., J. A. Leigh-Bell, H. Yu, P. Bertone, M. Gerstein, and M. Snyder.** 2006. Target hub proteins serve as master regulators of development in yeast. Genes Dev. **20:**435–448.
6. **Braun, B. R., M. van Het Hoogqq, C. d'Enfert, M. Martchenko, J. Dungan, A. Kuo, D. O. Inglis, M. A. Uhl, H. Hogues, M. Berriman, M. Lorenz, A. Levitin, U. Oberholzer, C. Bachewich, D. Harcus, A. Marcil, D. Dignard, T. Iouk, R. Zito, L., Frangeul, F. Tekaia, K. Rutherford, E. Wang, C. A. Munro, S. Bates, N. A. R. Gow, L. L. Hoyer, G. Kohler, J. Morschhäuser, G. Newport, S. Znaidi, M. Raymond, B. Turcotte, G. Sherlock, M. Costanzo, J. Ihmels, J. Berman, D. Sanglard, N. Agabian, A. P. Mitchell, A. D. Johnson, M. Whiteway, and A. Nantel.** 2005. A human-curated annotation of the *Candida albicans* genome. PLoS Genet. **1:**36–57.
7. **Care, R. S., J. Trevethick, K. M. Binley, and P. E. Sudbery.** 1999. The MET3 promoter: a new tool for *Candida albicans* molecular genetics. Mol. Microbiol. **34:**792–798.
8. **Caspari, T.** 1997. Onset of gluconate-H^+ symport in *Schizosaccharomyces pombe* is regulated by the kinases Wis1 and Pka1, and requires the *gti1*$^+$ gene product. J. Cell Sci. **110:**2599–2608.
9. **Daniels, K. J., T. Srikantha, S. R. Lockhart, C. Pujol, and D. R. Soll.** 2006. Opaque cells signal white cells to form biofilms in *Candida albicans*. EMBO J. **25:**2240–2252.
10. **Fonzi, W. A., and M. Y. Irwin.** 1993. Isogenic strain construction and gene mapping in *Candida albicans*. Genetics **134:**717–728.
11. **Gerami-Nejad, M., J. Berman, and C. A. Gale.** 2001. Cassettes for PCR-mediated construction of green, yellow, and cyan fluorescent protein fusions in *Candida albicans*. Yeast **18:**859–864.
12. **Halme, A., S. Bumgarner, C. Styles, and G. R. Fink.** 2004. Genetic and epigenetic regulation of the FLO gene family generates cell-surface variation in yeast. Cell **116:**405–415.
13. **Hartwell, L. H.** 1976. Sequential function of gene products relative to DNA synthesis in the yeast cell cycle. J. Mol. Biol. **104:**803–817.
14. **Hazan, I., and H. Liu.** 2002. Hyphal tip-associated localization of Cdc42 is F-actin dependent in *Candida albicans*. Eukaryot. Cell **1:**856–864.
15. **Heid, P. J., D. Wessels, K. J. Daniels, D. P. Gibson, H. Zhang, E. Voss, and D. R. Soll.** 2004. The role of myosin heavy chain phosphorylation in *Dictyostelium* motility, chemotaxis and F-actin localization. J. Cell Sci. **117:**4819–4835.
16. **Horak, C. E., and M. Snyder.** 2002. ChIP-chip: a genomic approach for identifying transcription factor binding sites. Methods Enzymol. **350:**469–483.
17. **Hull, C. M., and A. D. Johnson.** 1999. Identification of a mating type-like locus in the asexual pathogenic yeast *Candida albicans*. Science **285:**1271–1275.

18. **Iyer, V. R., C. E. Horak, C. S. Scafe, D. Botstein, M. Snyder, and P. O. Brown.** 2001. Genomic binding sites of the yeast cell-cycle transcription factors SBF and MBF. Nature **409:**533–538.
19. **Jones, T., N. A. Federspiel, H. Chibana, J. Dungan, S. Kalman, B. B. Magee, G. Newport, Y. R. Thorstenson, N. Agabian, P. T. Magee, R. W. Davis, and S. Scherer.** 2004. The diploid genome sequence of *Candida albicans*. Proc. Natl. Acad. Sci. USA **101:**7329–7334.
20. **Katan-Khaykovich, Y., and K. Struhl.** 2005. Heterochromatin formation involves changes in histone modifications over multiple cell generations. EMBO J. **24:**2138–2149.
21. **Klar, A., T. Srikantha, and D. R. Soll.** 2001. A histone deacetylation inhibitor and mutant promote colony-type switching of the human pathogen *Candida albicans*. Genetics **158:**919–924.
22. **Kunitomo, H., A. Sugimoto, C. R. Wilkinson, and M. Yamamoto.** 1995. *Schizosaccharomyces pombe* pac2$^+$ controls the onset of sexual development via a pathway independent of the cAMP cascade. Curr. Genet. **28:**32–38.
23. **Kvaal, C., S. A. Lachke, T. Srikantha, K. Daniels, J. McCoy, and D. R. Soll.** 1999. Misexpression of the opaque phase-specific gene *PEP1* (*SAP1*) in the white phase of *Candida albicans* confers increased virulence in a mouse model of cutaneous infection. Infect. Immun. **67:**6652–6662.
24. **Lan, C., G. Newport, L. A. Murillo, T. Jones, S. Scherer, R. W. Davis, and N. Agabian.** 2002. Metabolic specialization associated with phenotypic switching in *Candida albicans*. Proc. Natl. Acad. Sci. USA **99:**14907–14912.
25. **Lee, K. L., H. R. Buckley, and C. C. Campbell.** 1975. An amino acid liquid synthetic medium for the development of mycelial and yeast forms of *Candida albicans*. Sabouraudia **13:**148–153.
26. **Legrand, M., P. Lephart, A. Forsche, F.-M. C. Mueller, T. Walsh, P. T. Magee, and B. B. Magee.** 2004. Homozygosity at the *MTL* locus in clinical strains of *Candida albicans*: karyotypic rearrangements and tetraploid formation. Mol. Microbiol. **52:**1451–1462.
27. **Li, F., and S. P. Palecek.** 2005. Identification of *Candida albicans* genes that induce *Saccharomyces cerevisiae* cell adhesion and morphogenesis. Biotechnol. Prog. **21:**1601–1609.
28. **Lloyd, V. K., D. Dyment, D. A. Sinclair, and T. A. Grigliatti.** 2003. Different patterns of gene silencing in position-effect variegation. Genome **46:**1104–1117.
29. **Lockhart, S. R., K. J. Daniels, R. Zhao, D. Wessels, and D. R. Soll.** 2003. Cell biology of mating in *Candida albicans*. Eukaryot. Cell **2:**49–61.
30. **Lockhart, S. R., C. Pujol, K. Daniels, M. Miller, A. Johnson, and D. R. Soll.** 2002. In *Candida albicans*, white-opaque switchers are homozygous for mating type. Genetics **162:**737–745.
31. **Miller, M. G., and A. D. Johnson.** 2002. White-opaque switching in *Candida albicans* is controlled by mating-type locus homeodomain proteins and allows efficient mating. Cell **110:**293–302.
32. **Morrow, B., J. Anderson, E. Wilson, and D. R. Soll.** 1989. Bidirectional stimulation of the white-opaque transition of *Candida albicans* by ultraviolet irradiation. J. Gen. Microbiol. **135:**1201–1208.
33. **Morrow, B., H. Ramsey, and D. R. Soll.** 1994. Regulation of phase-specific genes in the more general switching system of *Candida albicans* strain 3153A. J. Med. Vet. Mycol. **32:**287–294.
34. **Park, Y. N., and J. Morschhäuser.** 2005. Tetracycline-inducible gene expression and gene deletion in *Candida albicans*. Eukaryot. Cell **4:**1328–1342.
35. **Ren, S., F. Robert, J. J. Wyrick, O. Aparicio, E. G. Jennings, I. Simon, J. Zeitlinger, J. Schreiber, N. Hannett, E. Kanin, T. L. Volkert, C. J. Wilson, S. P. Bell, and R. A. Young.** 2000. Genome-wide location and function of DNA binding proteins. Science **290:**2306–2309.
36. **Reuss, O., A. Vik, R. Kolter, and J. Morschhäuser.** 2004. The SAT1 flipper, an optimized tool for gene disruption in *Candida albicans*. Gene **341:**119–127.
37. **Rikkerink, E. H., B. B. Magee, and P. T. Magee.** 1988. Opaque-white phenotype transition: a programmed morphological transition in *Candida albicans*. J. Bacteriol. **170:**895–899.
38. **Sherman, F., G. R. Fink, and J. B. Hicks.** 1986. Laboratory course manual for methods in yeast genetics. Cold Spring Harbor Laboratory, Cold Spring Harbor, N.Y.
39. **Slater, M. L.** 1973. Effect of reversible inhibition of deoxyribonucleic acid synthesis on the yeast cell cycle. J. Bacteriol. **113:**263–270.
40. **Slutsky, B., M. Staebell, J. Anderson, L. Risen, M. Pfaller, and D. R. Soll.** 1987. "White-opaque transition": a second high-frequency switching system in *Candida albicans*. J. Bacteriol. **169:**189–197.
41. **Soll, D. R.** 1992. High frequency switching in *Candida albicans*. Clin. Microbiol. Rev. **5:**183–203.
42. **Soll, D. R.** 2003. *Candida albicans*, p. 165–201. *In* A. Craig and A. Scherf (ed.), Antigenic variation. Academic Press, Ltd., London, United Kingdom.
43. **Soll, D. R.** 2004. Mating-type locus homozygosis, phenotypic switching and mating: a unique sequence of dependencies in *Candida albicans*. Bioessays **26:**10–20.
44. **Soll, D. R., C. J. Langtimm, J. McDowell, J. Hicks, and R. Galask.** 1987. High frequency switching in *Candida* strains isolated from vaginitis patients. J. Clin. Microbiol. **25:**1611–1622.
45. **Srikantha, T., and D. R. Soll.** 1993. A white-specific gene in the white-opaque switching system of *Candida albicans*. Gene **131:**53–60.
46. **Srikantha, T., L. Tsai, K. Daniels, A. Klar, and D. R. Soll.** 2002. The histone deacetylase genes *HDA1* and *RPD3* play distinct roles in the regulation of high frequency phenotypic switching in *Candida albicans*. J. Bacteriol. **183:**4614–4625.
47. **Strauss, M. L., N. P. Jolly, M. G. Lambrechts, and P. van Rensburg.** 2001. Screening for the production of extracellular hydrolytic enzymes by non-*Saccharomyces* wine yeasts. J. Appl. Microbiol. **91:**182–190.
48. **Tavanti, A., A. D. Davidson, M. J. Fordyce, N. A. R. Gow, M. C. J. Maiden, and F. C. Odds.** 2005. Population structure and properties of *Candida albicans* as determined by multilocus sequence typing. J. Clin. Microbiol. **43:**5601–5613.
49. **Tsong, A. E., M. G. Miller, R. M. Raisner, and A. D. Johnson.** 2003. Evolution of a combinatorial transcriptional circuit: a case study in yeasts. Cell **115:**389–399.
50. **Wright, R., M. L. Parrish, E. Cadera, L. Larson, C. K. Matson, P. Garrett-Engele, C. Armour, P. Y. Lum, and D. D. Shoemaker.** 2003. Genes involved in endoplasmic reticulum biogenesis. Yeast **20:**881–892.
51. **Zettel, M. F., L. R. Garza, A. M. Cass, A. M., R. A. Myhre, L. A. Haizlip, S. N. Osadebe, D. W. Sudimack, R. Pathak, T. L. Stone, and M. Polymenis.** 2003. The budding index of *Saccharomyces cerevisiae* deletion strains identifies genes important for cell cycle progression. FEMS Microbiol. Lett. **223:**253–258.